Chin. Sci. Bull. (2014) 59(36):5290–5301
DOI 10.1007/s11434-014-0543-8

csb.scichina.com
www.springer.com/scp

Article

Condensed Matter Physics

# Synchrotron X-ray diffraction techniques for in situ measurement of hydride formation under several gigapascals of hydrogen pressure

**Hiroyuki Saitoh · Akihiko Machida · Katsutoshi Aoki**

Received: 18 January 2014 / Accepted: 23 April 2014 / Published online: 15 July 2014


**Abstract** The high-pressure technique is a fundamental tool for realizing novel phase transitions, chemical reactions, and other exotic phenomena. Hydrogenation is one example of a high-pressure reaction; at high pressures of several gigapascals, hydrogen becomes chemically active and reacts with metals and alloys to form hydrides. This paper covers a high-pressure study of the hydrogenation process and the synthesis of hydrides using a cubic-type multi-anvil apparatus. The experimental details of a hydrogenation cell assembly, high-temperature and high-pressure generation, and an in situ observation technique are presented. These experiments are conducted with the aid of in situ synchrotron radiation X-ray diffraction measurements operated in an energy-dispersive mode in the conventional manner for time-resolved measurements and a newly developed angle-dispersive mode for observation of the crystal growth process during formation of metal hydrides. Two successful cases of high-pressure hydrogenation are presented: aluminum hydride, $AlH_3$, and an aluminum-based alloy hydride, $Al_2CuH_x$, which are potential candidates for hydrogen storage materials.

SPECIAL TOPIC: High Pressure Physics

H. Saitoh (✉) · A. Machida
Quantum Beam Science Directorate, Japan Atomic Energy Agency, Sayo-cho, Sayo-gun, Hyogo 679-5148, Japan
e-mail: cyto@spring8.or.jp

K. Aoki
Institute for Materials Research, Tohoku University, Aoba-ku, Sendai 980-8577, Japan

**Keywords** Aluminum · Hydride · High pressure and high temperature · In situ measurement · Synchrotron radiation X-ray diffraction measurement

## 1 Introduction

Applying high pressure to a material enables us to effectively and significantly alter its volume and, consequently, its physical properties. We can induce phase transitions, chemical reactions, and other phenomena by applying high pressure in the gigapascal range. In this context, metal–hydrogen systems under high pressure have been intensively studied; highly pressurized hydrogen becomes significantly reactive owing to a steep increase in the chemical potential of hydrogen [1], and it reacts with metals to form novel hydrides stable only under high pressure. A large-volume high-pressure apparatus is a promising tool for such synthetic studies of metal hydrides, as it enables us to generate high pressures and high temperatures sufficient for the hydrogenation reaction and often allows us to recover a sufficient amount of synthesized hydrides for characterization at ambient conditions.

In the 1960s, Baranowski et al. [2, 3] initiated the study of high-pressure hydrogenation of metals using a piston–cylinder apparatus. They succeeded in hydrogenating pure nickel at around 1 GPa. Recently, the group members successfully synthesized novel hydrides of Laves phase intermetallic compounds using an improved piston–cylinder apparatus at a pressure of up to 1.2 GPa [4]. Subsequently, Antonov [5] developed a new technique for high-pressure hydrogenation. They use a Troid-type high-pressure apparatus, which contains a metal capsule filled with a metal sample and chemical hydrides as an internal hydrogen source. The high-pressure apparatus is designed to

allow rapid cooling of the synthesized hydrides to the temperature of liquid nitrogen; thermodynamically unstable hydrides can be recovered at ambient pressure conditions and used for precise structural study via neutron diffraction [6]. In the 1980s, Wakamori et al. [7] reported a high-pressure hydrogenation study using a cubic-type multi-anvil apparatus, in which a reaction vessel similar to that developed by the Russian group was used. Fukai et al. [8] reported a high-pressure study of a Fe–H system using a cubic-type multi-anvil apparatus. They later improved the high-pressure technique [9], and this improved technique has been widely used to synthesize novel hydrides, especially by Japanese groups [10–12]. A number of reviews of high-pressure hydrogenation studies are now available [1–3, 5].

In this paper, we describe our recent results for the hydrogenation of metals under high pressure and high temperature. Details of a cubic-type multi-anvil apparatus and hydrogenation cell assembly will be given. The formation and crystal structures of hydrides are investigated by in situ synchrotron radiation X-ray diffraction (SR-XRD) measurements. Two alternative measuring systems for X-ray diffraction will also be presented. Finally, successful results for the hydrogenation of aluminum (Al) and an aluminum-based alloy, $Al_2Cu$, are presented.

## 2 Experimental methods

### 2.1 Multi-anvil apparatus for high-pressure and high-temperature generation

A cubic-type multi-anvil apparatus is employed for generating high-pressure and high-temperature conditions up to 10 GPa and 1,000 °C, respectively. This high-pressure apparatus was developed by Osugi et al. [13], and its remodeled version has been widely used in materials and earth sciences. Figure 1 shows a schematic of the central part of the cubic-type multi-anvil apparatus, which consists of six anvils arranged in a cubic configuration to generate isostatic pressure on a cubic pressure medium. The opposing two anvils are pushed forward with a uniaxial hydraulic press and the remaining four anvils, mounted on wedge-shaped side blocks, are pushed in synchronously. Thin Teflon or glass epoxy sheets are attached to the sliding faces of the side blocks for electrical insulation and to reduce friction between the guide and side blocks. The cubic pressure medium is made larger than the anvil size so that the excess volume is extruded into gaps a few millimeters wide between the anvils to seal the pressurized sample inside the pressure medium. The pressure generation depends on the anvil size: ~6 GPa with 6-mm-edge anvils and ~10 GPa with 4-mm-edge anvils.

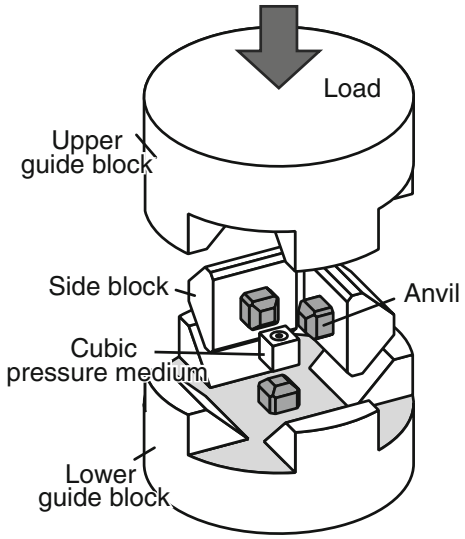


**Fig. 1** A schematic of a cubic-type multi-anvil apparatus

### 2.2 Hydrogenation reaction cell

The hydrogenation reaction cell was originally developed by Fukai and Okuma [9], and it has been successively modified for experimental purposes [10–12, 14]. A schematic of a high-pressure cell for synchrotron X-ray diffraction measurements is shown in Fig. 2. The first technical issue of the hydrogenation experiment is how to load hydrogen in a sample capsule. Hydrogen fluid or liquid can be loaded in a compact high-pressure apparatus such as diamond–anvil cell [15–17], but not in a large device such as a cubic-type multi-anvil apparatus. To provide a sufficient amount of hydrogen gas to completely hydrogenate a sample, it requires a dense hydrogen fluid, prepared via compression to 200 MPa, or liquid hydrogen formed by cooling below the boiling temperature of 20 K. Such a loading process is unavailable for the large apparatus.

Instead of gaseous hydrogen, solid chemical hydrides are used as the internal hydrogen sources. A powder mixture of $NaBH_4$ and $Ca(OH)_2$ (molar ratio 1:2) is conventionally used for this purpose. Since the decomposition temperature of $NaBH_4$ is high (400 °C at ambient pressure, and it increases with increasing pressure), the powdered mixture is used. $Ca(OH)_2$ is firstly decomposed into CaO and $H_2O$, and then, formed $H_2O$ reacts with $NaBH_4$ to evolve hydrogen (a hydrolysis reaction). The reaction paths are:

$$Ca(OH)_2 \rightarrow CaO + H_2O, \quad (1)$$

$$NaBH_4 + 2H_2O \rightarrow 4H_2 + NaBO_2. \quad (2)$$

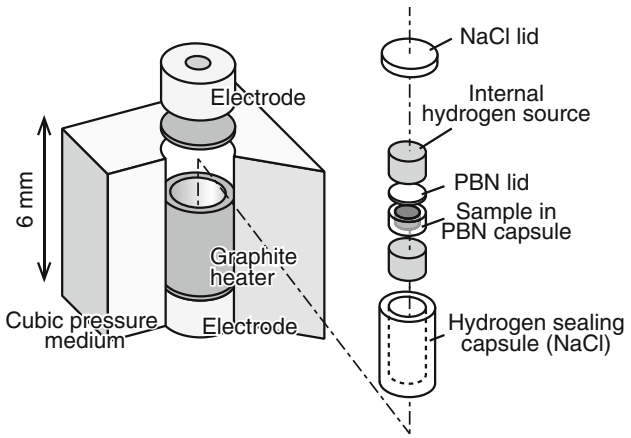


**Fig. 2** A high-pressure cell assembly for the hydrogenation experiment

The overall reaction is irreversible, and thus, evolved hydrogen is expected to be used only for a hydrogenation reaction of a sample. $LiAlH_4$ is also employed as an internal hydrogen source, depending on samples to be hydrogenated. Owing to the high chemical reactivity of hydrides to water, they are handled in an inert gas atmosphere, such as an argon gas environment. The internal hydrogen source is stable at ambient conditions and evolves hydrogen on heating to around 400 °C. Evolved hydrogen reacts with a sample in the hydrogen-sealing capsule. Disks of an internal hydrogen source, ~1.2 mm in diameter and 0.9 mm in height, are made by compaction of the powder and used to sandwich the sample capsule in the middle (see Fig. 2).

The sample capsule is made of pyrolytic boron nitride (PBN) (Shin-Etsu Chemical Co. Ltd., Japan). The PBN capsule allows hydrogen permeation, but blocks the by-products of the decomposed internal hydrogen sources. The sample is immersed and allowed to react with hydrogen to form hydrides. PBN has advantages over the standard boron nitride (BN) that is conventionally used. One advantage is its excellent machinability; the PBN capsule manufactured through milling has a half-mirror-like smooth surface that allows perfect removal of the sample from the capsule recovered after hydrogenation at high temperature and pressure. The coarse surface of standard BN adheres tightly to the sample surface, preventing them from separating. Another advantage of its machinability is that a thin-walled capsule and lid can be manufactured, because highly densified PBN is not friable. The thickness of the top and bottom PBN layers is 0.1 mm, which allows hydrogen to pass through quickly. The sample dimensions are typically 0.8 mm in diameter and 0.5 mm in height. The capsule containing the sample and disks of the hydrogen source are placed in a hydrogen-sealing capsule made of sodium chloride (NaCl).

The second technical issue is how to confine hydrogen in the high-pressure cell for a typical reaction time of 24 h. Metals with low hydrogen affinity are used to confine the hydrogen gas around the ambient pressure; however, they do not work well at higher pressures of several gigapascals, owing to the significant increase in hydrogen solubility of metals with pressure [18]. For example, aluminum has a very low hydrogen solubility, and hydrogen storage vessels made of aluminum alloys are mounted in fuel cell vehicles. The solubility of the hydrogen-resistant metal, however, increases from $x \approx 10^{-6}$ at 0.1 MPa to $x \approx 10^{-2}$ at 10 GPa around 800 °C. Other hydrogen-resistant metals show similar behaviors at high pressures, absorbing considerable amounts of hydrogen to form solid solutions or hydrides. Fukai and Okuma [9] have found that a NaCl capsule can confine hydrogen even at high pressures of several gigapascals. The NaCl capsule is confirmed to work well at 10 GPa and 800 °C for over 24 h [19]. Reagent-grade NaCl powder is ground with a mortar and pestle to make a fine powder with a particle size less than 5 μm. The fine powder is pelletized into a disk of the desired size, and then, the disk is shaped into a cylindrical capsule via milling.

The NaCl hydrogen-sealing capsule is inserted in a cylindrical heater made of graphite designed to generate high temperatures. The top and bottom ends of the heater are electrically contacted with metal electrodes to the top and bottom anvils, which are connected to an electric power supply through the top and bottom guide blocks. The generated temperature inside the NaCl capsule is calibrated with thermocouples embedded in a dummy sample to obtain the relationship between temperature and electric power. The hydrogenation experiment is conducted without thermocouples in order to reliably confine hydrogen in the capsule. The sample temperature is estimated using the calibration curve.

The cell components are placed in a straight hole in a cubic pressure medium made of pyrophyllite. The cube is baked in advance at 1,000 °C for 2 h; the heat-treated cube becomes slightly harder by dehydration, enabling us to generate pressures approximately 10 % higher than in the raw pyrophyllite cube. The high-pressure cell is assembled in a glove box filled with argon gas to avoid degradation of the internal hydrogen sources, which can react with water in air. The assembled cell is placed on the cubic-type multi-anvil apparatus and squeezed by synchronously moving the six anvils. Pressure is estimated based on the relationship between generated pressure and the applied load. The relationship is calibrated in advance via SR-XRD measurements for standard pressure markers such as NaCl, and the pressures are calculated from the lattice volumes using the equation of state reported in the literature [20].

### 2.3 In situ synchrotron radiation X-ray diffraction measurement in an energy-dispersive mode

The SR-XRD technique enables us to obtain structural information on the sample in situ under high-pressure and high-temperature conditions. An energy-dispersive X-ray diffraction (EDXD) technique is primarily used with a cubic-type multi-anvil apparatus, whereas an angle-dispersive X-ray diffraction (ADXD) technique, a conventional technique used in an ordinary X-ray diffractometer, is rarely employed. The cubic-type multi-anvil apparatus allows limited optical windows for incident and diffracted X-rays, but it does not allow the wide-angle scanning required for ADXD measurement. The point detection of diffracted X-rays via the EDXD method has great advantages for measuring diffraction profiles quickly using a multi-anvil apparatus with spatial limitations.

Figure 3 depicts a schematic of the experimental setup. The incident beam—white X-rays from a synchrotron radiation light source—passes through a narrow gap (200–300 μm) between the side anvils and irradiates the sample compressed in the high-pressure cell. The X-rays diffracted from the sample are guided through a narrow gap between the anvils on the opposite side and are detected by a solid-state detector fixed at an appropriate angle of 4°–10° off from the incident beam axis. The BL14B1 beam-line at SPring-8 provides X-ray energies ranging from 30 to 120 keV for the in situ diffraction measurement [21]. This energy range corresponds to $d$ values of 1–3.5 Å for a fixed diffraction angle of 6°. The typical acquisition time is 15–120 s per profile. A collimator is placed between the sample and the detector to collect X-rays diffracted from the sample alone.

### 2.4 In situ synchrotron radiation X-ray diffraction measurement in an angle-dispersive mode

The EDXD method allows for quick collection of powder X-ray diffraction profiles from a very limited reciprocal lattice space. The reciprocal lattice space observable in the EDXD mode is very limited, as illustrated in Fig. 4a. When the grain size of the sample is larger than approximately 20 μm, some sets of reciprocal lattice points $hkl$ do not intersect with the Ewald sphere and hence do not satisfy the Bragg condition for diffraction. Their diffraction peaks are lost in the measurement of the EDXD mode. We cannot obtain reliable or accurate diffraction data by the EDXD mode for the sample with the large grain size.

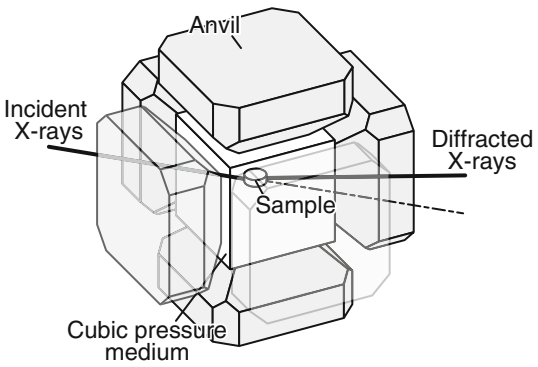


**Fig. 3** A schematic of the experimental setup of the in situ synchrotron radiation X-ray diffraction measurement in the energy-dispersive mode

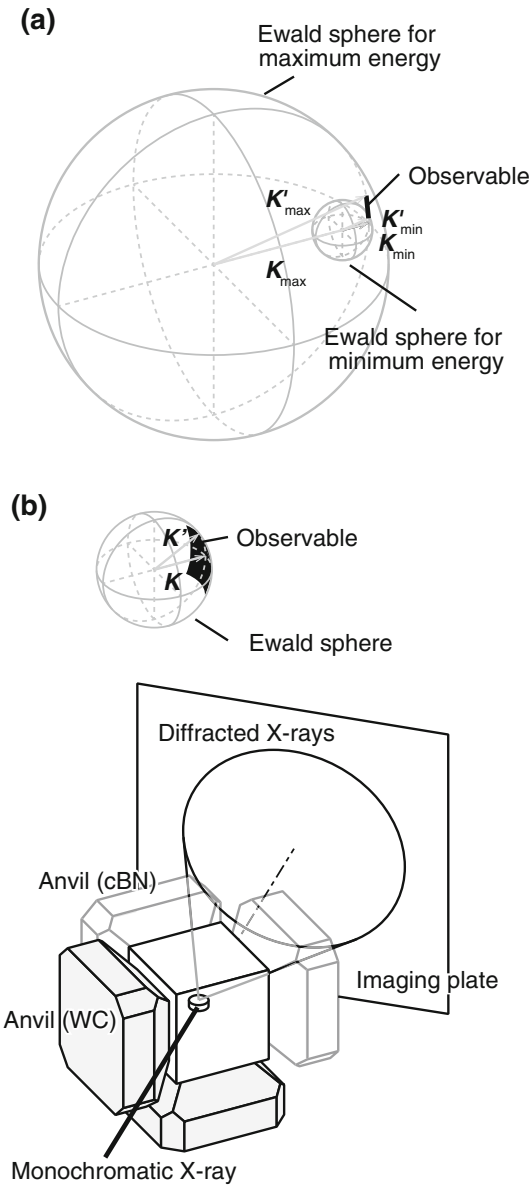


**Fig. 4** **a** The observable reciprocal lattice space in the energy-dispersive mode. Vectors $\boldsymbol{K}$ and $\boldsymbol{K}'$ show the directions of the incident and diffracted X-rays. The energies of the incident X-rays for $K_{\min}$ and $K_{\max}$ are 30 and 120 keV, respectively. **b** The observable reciprocal lattice space in the angle-dispersive mode with an incident X-ray energy of 60 keV and a schematic of its experimental setup

In contrast to the one-point detection in the EDXD mode, a two-dimensional imaging plate detector is used in the ADXD mode. Anvils made of cubic boron nitride (cBN), which are transparent to X-rays, allow for the collection of whole diffraction rings, or Debye rings, from the sample even with large grains or preferred orientations [22–24]. ADXD allows further evaluation of the average grain size of the sample from the number of diffraction spots observed (note that if the sample is fine powder, the average grain size can be determined from the observed peak width using the Scherre formula, which is independent of the detecting mode [25]). Figure 4b shows a schematic of the ADXD measurement system and its observable reciprocal lattice space. The two lateral anvils on the detector side are replaced by those made of cBN, through which the diffracted X-rays from the sample can pass to arrive at the imaging plate detector. Uniform Debye rings are recorded for an ideal powder sample, while sharp Bragg spots are observed for a sample with a large grain size.

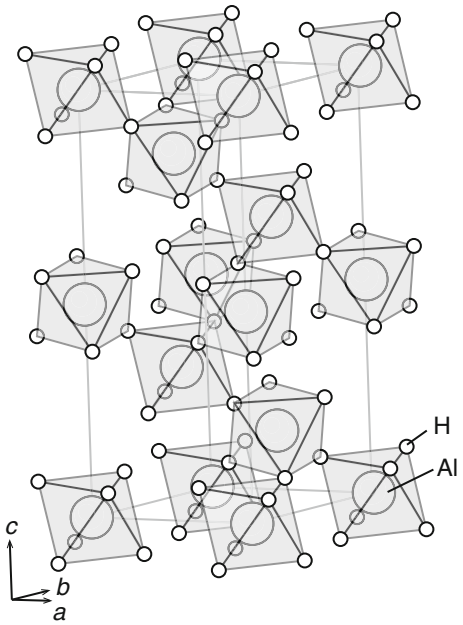


**Fig. 5** A crystal structure of $AlH_3$

## 3 Hydrogenation of aluminum

### 3.1 Background

Aluminum tri-hydride ($AlH_3$) is a crystalline solid at ambient conditions [26]. $AlH_3$ has a large gravimetric and volumetric hydrogen content (10.1 wt% and 148 kg/m$^3$, respectively) and therefore has been studied as a potential hydrogen storage material [26–29]. $AlH_3$ can be prepared by organometallic synthesis procedures as a kinetically stabilized solid that displays excellent stability even in air. Seven polymorphs of $AlH_3$ have been obtained through organometallic synthesis [30]. Pressure-induced structural phase transformations have also been investigated [31]. A metallic phase with a simple cubic structure has been found above 100 GPa. The α-phase, which crystallizes in a trigonal space group R-3c with six molecules in a hexagonal unit cell of dimensions $a = 4.449$ Å and $c = 11.804$ Å [30], is the most stable phase below 10 GPa; its crystal structure is shown in Fig. 5. The crystal structure consists of corner-shearing $AlH_6$ octahedra. Only the α-phase is discussed in this section.

At atmospheric pressure, $AlH_3$ cannot be obtained from a metallic element, as the hydrogenation reaction of pure aluminum has not been realized; pure aluminum is expected to be hydrogenated above 0.7 GPa and room temperature, where $AlH_3$ is thermodynamically stable. However, the hydrogenation reaction is inhibited even in the $AlH_3$-stable conditions because the surface oxide layer on aluminum prevents reaction. Tkacz et al. [32] have reported a re-hydrogenation reaction of decomposed $AlH_3$ at 2.8 GPa. Konovalov and Bulychev [33] have observed the dehydrogenation of $AlH_3$ and its re-hydrogenation reactions via differential thermal analysis and have determined the pressure–temperature relation of $AlH_3$, in which they used $AlH_3$ as a starting material. These early hydrogenation and dehydrogenation experiments [32, 33] revealed decomposition temperatures approximately 100 °C higher than those obtained through thermodynamical calculations. Graetz et al. [26] and Sakharov et al. [34] have also reported the pressure–temperature relation of $AlH_3$, determined by using non-oxidized aluminum powder prepared by the dehydrogenation of $AlH_3$ and filled in a copper capsule. Their results are consistent with the thermodynamical calculations. They conjectured that the earlier works were affected by an oxide layer virtually impermeable to hydrogen. Kato et al. [35] have reported that the surface oxide layer of $AlH_3$ prevents the dehydrogenation reaction of $AlH_3$ using in situ X-ray photoelectron spectroscopy. It has been clarified that both the hydrogenation of aluminum and the dehydrogenation of $AlH_3$ are prevented by a surface oxide layer. It is thought that the hydrogenation of pristine aluminum is difficult even under thermodynamically stable conditions for $AlH_3$.

Apart from hydrogen storage applications, the hydrogenation reaction of aluminum is worth investigating, because the hydrogenation reaction process of aluminum is expected to be different from other hydrogen-absorbing metals and alloys. Aluminum metal hardly absorbs hydrogen in the interstitial sites of the metal lattice (e.g., H/Al $\approx 10^{-1}$ at 10 GPa and 1,250 °C [18]).

Hydrogenation of aluminum does not produce mono- and di-hydrides; only tri-hydride $AlH_3$ is formed, whereas rare-earth metals and hydrogen-absorbing alloys form solid–solution phases and low- and high-hydrogen content phases. The volume of the aluminum metal lattice doubles in size as a result of the hydrogenation reaction ($\Delta v = 5.6$ Å$^3$ per H atom). The lattice expansion is significantly larger than that of other metals and alloys ($\Delta v = 2$–$3$ Å$^3$ per H atom) [1].

We have reported that pristine aluminum with a surface oxide layer can be hydrogenated above 8.9 GPa and 600 °C [14]. The reaction process has been investigated using in situ SR-XRD measurements. It has been clarified that the oxide layer on aluminum is partly removed or modified by the high-pressure and high-temperature hydrogen fluid, which enables us to achieve a hydrogenation reaction of aluminum and investigate the process.

### 3.2 In situ observation by the EDXD method

Figure 6 shows a series of X-ray diffraction profiles taken during a hydrogenation of aluminum and a dehydrogenation of the produced $AlH_3$. The starting material was pure aluminum, in disks 0.8 mm in diameter and 0.05 mm in thickness. The disks were stacked to fill the sample capsule. The sample was used as received without any treatment to remove the oxide layer. An X-ray photoelectron spectroscopy measurement reveals that the oxide layer was 35-Å thick. The sample is pressurized to 10 GPa at room temperature, heated to 650 °C, and then kept in hydrogen fluid. Bragg peaks from pure aluminum, BN, and NaCl are observed just after the sample is heated to 650 °C (Fig. 6a). New Bragg peaks appear approximately 20 min after the sample is heated to 650 °C. These peaks are weak when they appear and grow upon continued heating. These peaks are clearly seen about 200 min after heating, as shown in Fig. 6b. They are indexed with a trigonal unit cell of $AlH_3$, indicating that pristine aluminum is successfully hydrogenated at 10 GPa and 650 °C. Then, the sample is heated to 800 °C. The Bragg peaks from $AlH_3$ vanish (Fig. 6c). The produced $AlH_3$ decomposes into aluminum and hydrogen. The aluminum is hydrogenated again on successive cooling to 650 °C (Fig. 6d). The hydrogenation of aluminum and dehydrogenation of the produced $AlH_3$ are realized and observed in situ through SR-XRD measurements. It is worth mentioning that the crystal sizes of $AlH_3$ and their crystal directions change during the hydrogenation and dehydrogenation cycle. This is because the relative intensities of diffraction from $AlH_3$ change even though the diffraction profiles are taken from the same sampling spot.

The hydrogenation and dehydrogenation pressure–temperature conditions are determined based on the in situ measurement and summarized in the inset of Fig. 6. It

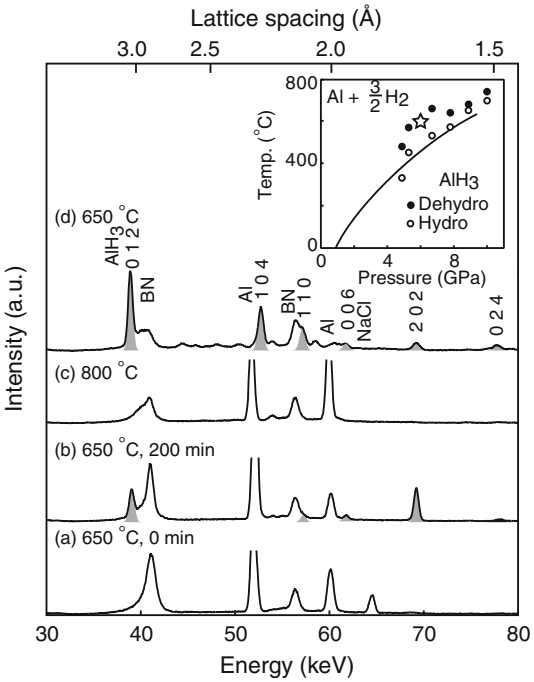


**Fig. 6** A series of X-ray diffraction profiles taken during the hydrogenation of aluminum and dehydrogenation of the produced $AlH_3$. The *shaded Bragg peaks* are from $AlH_3$. The *inset* summarizes hydrogenation and dehydrogenation pressure–temperature conditions

should be noted that a high pressure of over 8.9 GPa is necessary for initial hydrogenation of passivated aluminum. However, aluminum obtained by dehydrogenation of the produced $AlH_3$ can be hydrogenated at less than 8.9 GPa, as reported previously [32–34]. The pressure–temperature conditions are determined by decreasing the pressure from 10 to 4.5 GPa. Our results agree with the equilibrium curve obtained by thermodynamical calculations. Sakharov et al. [34] have pointed out that the oxide layer on aluminum exhibits an artificially high decomposition temperature compared with that at equilibrium. Our results imply that the oxide layer on aluminum is partly removed or modified by the high-pressure and high-temperature hydrogen fluid, which enables us to hydrogenate pristine aluminum and determine decomposition temperatures free from the kinetic effects caused by the surface oxide. It is difficult to observe the oxide layer under high pressure, and thus the modification of the surface oxide layer has yet to be observed.

We infer that the modification of the surface oxide layer is irrelevant to the hydrogenation reaction. If this is true, then the modification may occur in $AlH_3$-unstable conditions (e.g., the pressure–temperature conditions indicated by a star in the inset of Fig. 6). Once the oxide layer on aluminum is modified (hereafter we refer to this treatment as the modifying treatment), the aluminum is not passivated again because the sample capsule is free from oxygen

unless the sample is recovered at ambient conditions. Aluminum modified in $AlH_3$-unstable conditions is expected to be hydrogenated by successive cooling into $AlH_3$-stable conditions.

The above presumption is experimentally confirmed [19]. Pristine aluminum is heated to 600 °C at 6 GPa in a hydrogen fluid. The sample is not hydrogenated at these pressure–temperature conditions because $AlH_3$ is thermodynamically unstable. After the sample is heated to 600 °C, the sample is immediately cooled to 400 °C, kept in a hydrogen fluid for 2 h, and recovered at ambient conditions. An optical microscope measurement reveals that $AlH_3$ is formed via the synthetic procedure. When pristine aluminum is immersed in a hydrogen fluid at 600 °C at 6 GPa without the modifying treatment, the sample is not hydrogenated (as mentioned above, a high pressure and high temperature of over 8.9 GPa and 600 °C are necessary for the initial hydrogenation reaction of pristine aluminum). It is confirmed that the modifying treatment enables pristine aluminum to be hydrogenated.

### 3.3 $AlH_3$ obtained by the hydrogenation reaction under high pressure

Figure 7 shows an optical micrograph of the recovered $AlH_3$ synthesized at 10 GPa and 650 °C for 24 h. The surface of the sample is covered with grains of $AlH_3$, while the inner part remains unreacted. The thickness of the produced $AlH_3$ is from 20 to 50 μm. Hydrogenation at the inner part of the aluminum is inhibited owing to slow hydrogen diffusion in the produced $AlH_3$; this $AlH_3$ prevents further hydrogenation of the inner part. The introduction of hydrogen permeation pathways allows the hydrogenation reaction of the inner part. Details of this are described elsewhere [36].

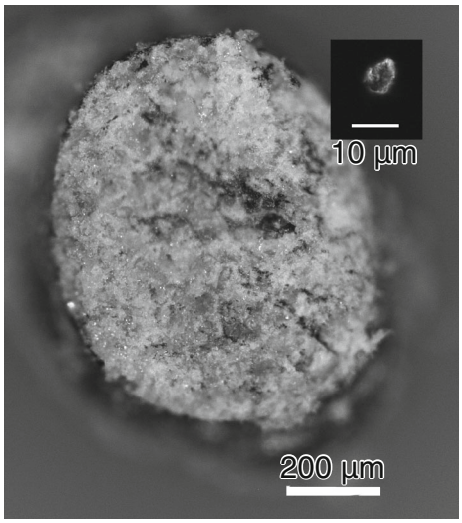


**Fig. 7** A polarized photomicrograph of the recovered $AlH_3$. The *inset* shows a transparent polarized photomicrograph of a particle of the produced $AlH_3$

The majority of the produced $AlH_3$ is composed of small crystalline particles less than a few microns in length. A few transparent particles exceed 10 μm in length (see the inset of Fig. 7). One of the transparent particles is characterized by taking an X-ray oscillation photograph of it in an undulator beam-line, BL22XU, at SPring-8. All the Bragg spots are sharp without peak splitting and indexed with a trigonal unit cell of $AlH_3$, indicating that the particle is a highly crystalline single crystal. The results raise the question of how such high-quality single crystals can grow through hydrogenation, given the significant modification in unit cell structure from cubic to trigonal and the accompanying volume expansion of the host metal lattice ($\Delta v/v = 100$ %). To clarify the crystal growth process of $AlH_3$, the hydrogenation reaction of aluminum is investigated through ADXD, which provides information about the crystal growth process.

### 3.4 Formation and crystal growth process of $AlH_3$ under high pressure

The starting material was pure aluminum disks, which were the same as those used for the EDXD measurement. Figure 8 summarizes ADXD images recorded on an imaging plate. Figure 8a is taken at 10 GPa and room temperature prior to heating. Uniform Debye rings from the aluminum sample are observed, indicating that the grain size of the sample is less than 1 μm (the relationship between the grain size and the number of Bragg spots are determined in advance by recovery experiments). The sample is heated to 600 °C at 10 GPa.

The uniform Debye rings from the sample change into brilliant Bragg spots just after the sample is heated to 600 °C (Fig. 8b). Solid-state grain growth of aluminum takes place. The grain size is 20–30 μm in length. Such solid-state grain growth is frequently observed at high pressure and high temperature [22].

The aluminum grains are slowly pulverized prior to the hydrogenation reaction of aluminum. The diffraction intensities of aluminum begin to decrease, and the Bragg spots are crushed into arc streaks after a 3-h heating treatment in hydrogen (Fig. 8c). Weak Debye rings of aluminum are also observed. These changes in the diffraction pattern indicate that aluminum grains are pulverized into small grains. It is worth mentioning that the pulverization is observed only in the $AlH_3$-stable pressure–temperature conditions. When the aluminum is kept in hydrogen at 10 GPa and 800 °C, which are outside of the $AlH_3$-stable conditions, the aluminum grains grown by

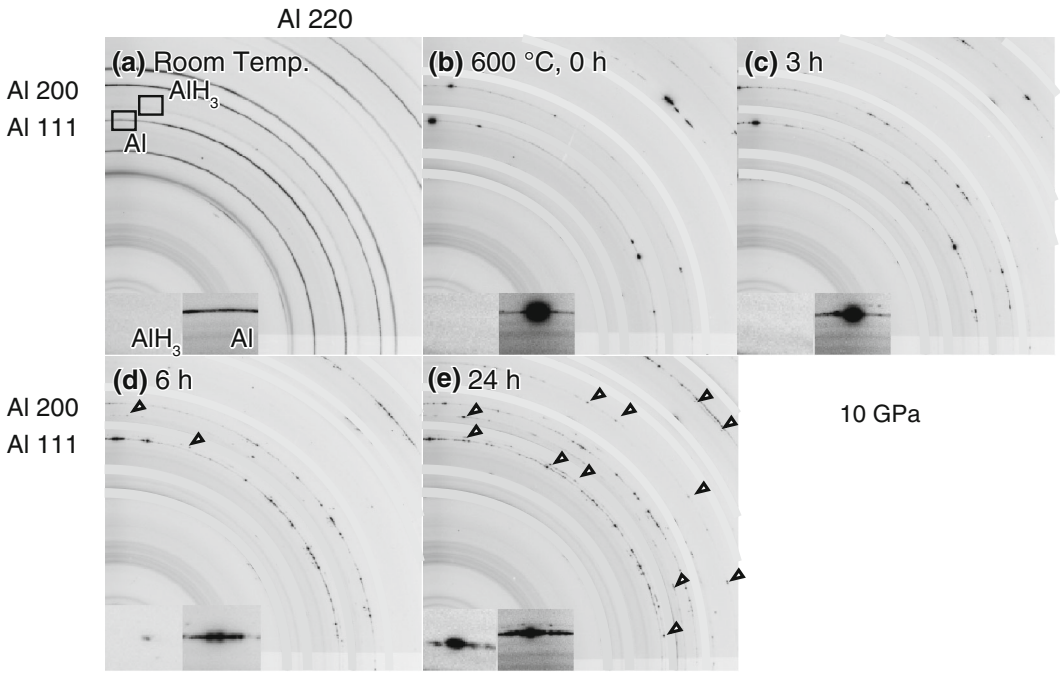


**Fig. 8** A series of recorded diffraction images in the angle-dispersive X-ray diffraction mode. Diffraction rings with *triangles* are from produced $AlH_3$. Diffraction rings without notations in **a** are from the sample capsule and the hydrogen-sealing capsule, and are masked in **b**–**e**

solid-state grain growth remain; no pulverization takes place.

The hydrogenation reaction does not cause the pulverization reaction directly, because hydrogenation reaction does not occur when the pulverization begins. This is in contrast to pulverization reactions observed for other hydrogen-absorbing alloys [37]. Pulverizations of other hydrides are thought to be caused by internal strain introduced by the large volume changes associated with the hydrogenation reactions.

The hydrogenation reaction of aluminum proceeds gradually, following the pulverization reaction. As seen in Fig. 8d, Bragg spots from $AlH_3$ begin to appear 6 h after heating. The grain size of $AlH_3$ is comparable to that of pulverized aluminum at this stage. The Bragg spots of $AlH_3$ become stronger and new Bragg peaks of $AlH_3$ appear simultaneously with continued heat treatment, as shown in Fig. 8e. Solid-state grain growth of $AlH_3$ and the hydrogenation reaction of aluminum to produce $AlH_3$ occur simultaneously. Finally, single crystals of $AlH_3$ 10–20 μm in length are formed.

The ADXD measurement on the aluminum–hydrogen system at 10 GPa and 600 °C has revealed the self-pulverization of aluminum prior to hydrogenation and the subsequent solid-state grain growth of $AlH_3$. The pulverization appears to be the precursor of the hydrogenation reaction because it occurs at pressure–temperature conditions where $AlH_3$ is thermodynamically stable. A hydrogen absorption or a reaction in aluminum must occur before the pulverization and cause it, though the absorption or the reaction has not been detected. Such a pulverization reaction has not been observed for other metals and alloys. SR-XRD studies of the hydrogenation processes of aluminum and other metals are currently being planned to clarify the origin of the pulverization reaction.

## 4 Synthesis of novel aluminum-based interstitial hydride

Not only pure aluminum hydride, $AlH_3$, but also aluminum-based hydrides are promising hydrogen storage materials for fuel cell vehicles because aluminum is lightweight and the most abundant metal in the Earth's crust. In this context, complex aluminum hydrides, such as $NaAlH_4$ and $LiAlH_4$, have been studied; however, because of their thermodynamical properties and slow kinetics, complex aluminum hydrides obtained so far are unsuited for practical applications. Apart from complex aluminum hydrides, few aluminum-based alloy hydrides have been reported. If such a material is developed, then it would expand the variety of aluminum-based hydrides.

Recently, we have demonstrated the formation of an aluminum-based interstitial hydride, $Al_2CuH_x$ [38]. The hydride formed can be recovered at ambient conditions and is characterized via a conventional X-ray diffraction

measurement. The interstitial nature of the hydride is investigated here.

Figure 9a shows a schematic of the crystal structure of the $Al_2Cu$ alloy. The alloy crystallizes in the space group I4/mcm with $a = 6.067$ Å and $c = 4.877$ Å [39]. An $Al_8Cu$ square antiprism is the structural unit of the crystal structure. One-dimensional chains are formed in the $c$ axis direction by face-sharing of $Al_8Cu$. These chains share edges to form a crystal structure with interstices. The starting material was ground $Al_2Cu$ alloy (particle size $< 50$ μm), which was made by arc-melting around ambient pressure. The sample was placed into a high-pressure cell, pressurized to 10 GPa, and then heated in hydrogen fluid. Structural changes and the hydrogenation reaction of the alloy were observed in situ via SR-XRD measurements in the EDXD mode.

Figure 10 plots X-ray diffraction profiles taken during the high-pressure and high-temperature treatment. The $Al_2Cu$ structure is maintained when the sample is pressurized at room temperature and heated to 600 °C in hydrogen fluid (Fig. 10a). The sample decomposes into $AlCu_{1.5}$ and aluminum at 880 °C on subsequent heating.

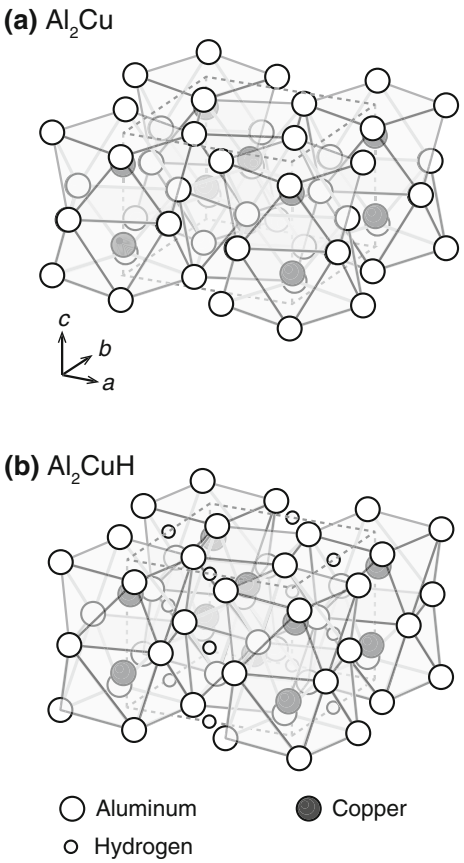


**Fig. 9** **a** Crystal structure of $Al_2Cu$ alloy. **b** Crystal structure of $Al_2CuH_x$. The positions of hydrogen atoms are determined by first-principles calculations

Figure 10b shows a diffraction profile taken at 900 °C after the decomposition. After decomposition, the sample is cooled to 800 °C. Figure 10c shows a diffraction profile taken at 800 °C, which is different from those of $Al_2Cu$, $AlCu_{1.5}$, and aluminum. The Bragg peaks in Fig. 10c are indexed with an enlarged unit cell of $Al_2Cu$, indicating volume expansion caused by a hydrogenation reaction of $Al_2Cu$.

The hydrogenation reaction proceeds only after the sample is decomposed into $AlCu_{1.5}$ and aluminum at 880 °C. $Al_2CuH_x$ is not formed when the sample is initially heated from room temperature to 800 °C in hydrogen fluid. This is probably because the surface oxide layer on the $Al_2Cu$ alloy prevents the hydrogenation reaction. The oxide layer is removed by the decomposition reaction, which allows the hydrogenation reaction on subsequent cooling of the sample. Such a complex temperature path for the hydrogenation reaction is difficult to explore without the aid of in situ SR-XRD measurements. It is worth mentioning that the melting temperatures [40] of aluminum (1,200 °C at 10 GPa), copper (1,400 °C at 10 GPa), and binary alloys increase with increasing pressure. A melting component is not detected during measurement, and it does not affect the hydrogenation process.

The produced hydride is quenched at ambient conditions. Hydrogen evolution from the recovered sample is observed around 150 °C at ambient pressure. A powder X-ray diffraction measurement reveals that the sample has an $Al_2Cu$ structure after the hydrogen evolution occurs. It

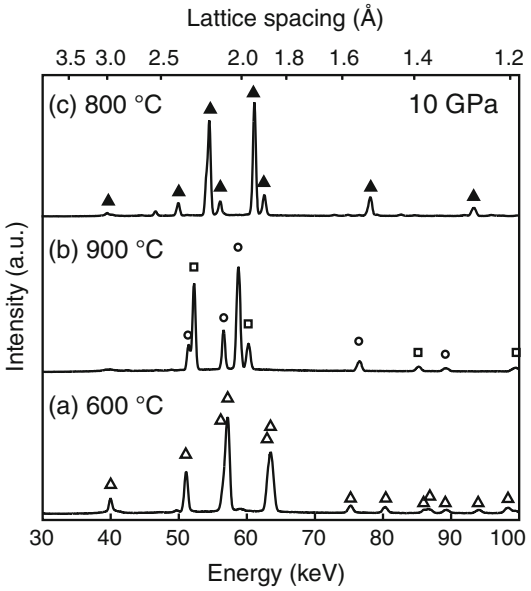


**Fig. 10** A series of X-ray diffraction profiles taken at 10 GPa and (*a*) 600 °C, (*b*) 900 °C, and (*c*) 800 °C. *Open triangles*, *closed triangles*, *circles*, and *squares* indicate Bragg peaks from $Al_2Cu$, $Al_2CuH_x$, $AlCu_{1.5}$, and aluminum, respectively

is clarified that the $Al_2CuH_x$ is formed through the hydrogenation reaction of the $Al_2Cu$ alloy at 10 GPa and 800 °C. The hydrogen content is roughly estimated to be $x \approx 1$ on the basis of mass measurements made during the dehydrogenation reaction, although the small sample volume of $< 0.2$ mm$^3$ does not allow a precise determination of the hydrogen content.

A powder X-ray diffraction profile of the recovered sample is shown in Fig. 11. Bragg peaks from $Al_2CuH_x$ are indexed using a tetragonal unit cell with $a = 6.110$ Å and $c = 5.201$ Å, an enlarged unit cell of the $Al_2Cu$ alloy. Some peaks from unreacted $Al_2Cu$, $AlCu_{1.5}$, and aluminum are detected from the recovered sample. The reaction yield is estimated to be approximately 60 % from a comparison of the diffraction intensities. The unit cell expands along the $c$ axis ($\Delta c/c = 7$ %) upon hydrogenation, whereas the lattice parameter $a$ remains almost unchanged ($\Delta a/a = 1$ %). The unit cell volume increases by 8 %, which is in accordance with the estimated hydrogen content of $x \approx 1$.

The diffraction profile of $Al_2CuH_x$ is reproduced by introducing twists of the $Al_8Cu$ square antiprisms around the $c$ axis. The peak intensities of $Al_2CuH_x$ are not reproduced with the simply enlarged unit cell of $Al_2Cu$ alloy, as seen in Fig. 11b. Here, we attempt to find a structure model of $Al_2CuH_x$ that reproduces the peak intensities. The space group is fixed to I4/mcm, and only the atomic parameter of aluminum is changed to find the model. The obtained crystal structure is shown in Fig. 9b (note that the positions of hydrogen atoms are determined only via first-principles calculations; details will be described later). The simulated X-ray diffraction profile for the obtained model is shown in Fig. 11a. It can be seen that the simulated profile agrees well with the experimentally observed one. The changed atomic parameter corresponds to a twist of the $Al_8Cu$ square antiprisms, which is illustrated in Fig. 12. The angle $\alpha$ (49.6° for $Al_2Cu$) between the corner-shared squares of aluminum atoms changes to $\alpha' = 66.1° \pm 0.5°$ as a result of the twist caused by the hydrogenation reaction.

Structural optimization via first-principles calculations is performed to examine the obtained structural model of $Al_2CuH_x$. The hydrogen content $x$ is fixed to be 1.0. The obtained structure is of an $Al_2Cu$-type with lattice parameters of $a = 6.137$ Å, $c = 5.225$ Å, and $\alpha' = 68.2°$, which are consistent with the experimentally determined values.

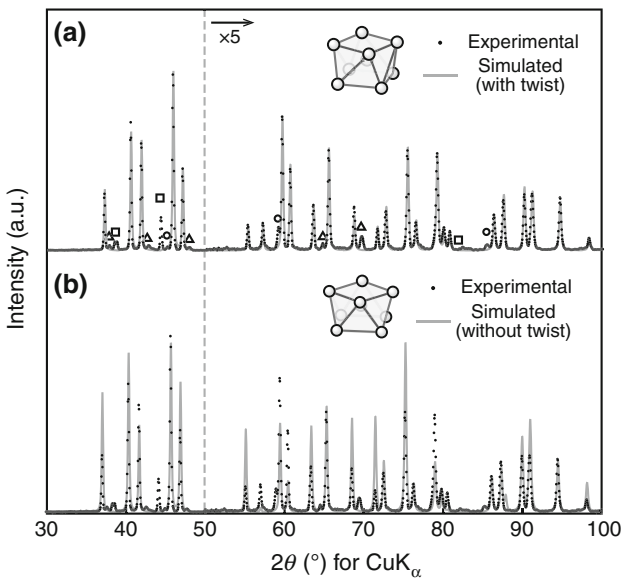


**Fig. 11** **a** A powder X-ray diffraction profile of the recovered sample with a simulated diffraction pattern made by introducing twists of the $Al_8Cu$ square antiprism. **b** A powder X-ray diffraction profile of the recovered sample with a simulated pattern without the twist. *Triangles*, *circles*, and *squares* indicate Bragg peaks from $Al_2Cu$, $AlCu_{1.5}$, and aluminum, respectively. Diffraction intensities above $2\theta = 50°$ are multiplied by a factor of 5

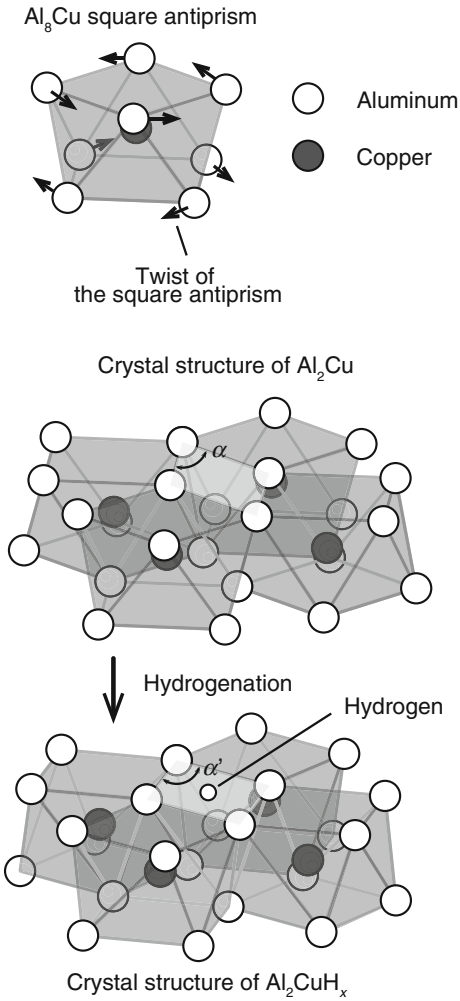


**Fig. 12** A schematic drawing of the crystal structures of $Al_2Cu$ and $Al_2CuH_x$ showing atomic movement during the hydrogenation reaction

This agreement supports both the validity of the structural model and the estimated hydrogen content, $x \approx 1$. Hydrogen atoms are located in the centers of the rhombuses of aluminum atoms, which are enlarged by the hydrogenation reaction as shown in Fig. 12. Hydrogen atoms are aligned linearly along the $c$ axis, as shown in Fig. 9b.

The structural change of the $Al_2Cu$ alloy caused by the hydrogenation reaction can be explained as follows. The $Al_8Cu$ square antiprisms are twisted to enlarge the interstitial spaces consisting of four aluminum atoms. Hydrogen atoms are located at the center of the enlarged interstitial site to form interstitial hydride, $Al_2CuH_x$ ($x \approx 1$). It is likely that the twist enables the formation of the interstitial hydride without lattice expansions of the $a$ and $b$ axes, whereas the unit cell is enlarged along the $c$ axis.

Interstitial hydrides are expected to exhibit different properties than those of complex aluminum hydrides. The properties of interstitial hydrides are favorable for hydrogen storage because the hydrogenation and dehydrogenation reactions would proceed simply and their thermodynamic properties are tunable by the addition of other elements to the alloy. Both the experimentally and theoretically obtained results are useful for exploring other aluminum-based interstitial hydrides. These findings will help expand the variety of aluminum-based alloy hydrides, which, in turn, will help in developing practical hydrogen storage materials.

## 5 Conclusions and future perspectives

This paper presented the latest advancement in the high-pressure study of the hydrogenation process of metals and alloys. The SR-XRD technique combined with the high-pressure technique using a cubic-type multi-anvil apparatus was shown to be a very powerful tool for in situ measurements, providing information on the synthetic conditions of novel metal hydrides and the reaction process. Examples of the hydrogenation of aluminum and aluminum-based alloys were successfully demonstrated via X-ray diffraction results. The X-ray diffraction measurement, however, indicates the limitations of the experiment, yielding structural information only on the metal atoms and no useful information on the hydrogen atom. This is because X-ray scattering from hydrogen atoms is too small compared with that from metal atoms, hardly contributing to diffraction profiles. The exact locations and stoichiometry of the hydrogen atoms in the hydrides remain unknown.

A neutron diffraction measurement would overcome the lack of hydrogen information in X-ray diffraction. The scattering from the nucleus of deuterium, an isotope of hydrogen, has sufficient intensity for diffraction measurements. A neutron diffractometer, PLANET, used for high-pressure experiments constructed at J-PARC, Japan [41, 42], allows us to make in situ measurements of the atomic positions and proportions of deuterium (hydrogen) in hydrides. However, neutron diffraction measurements require measuring times of up to several hours, even with high-intensity pulsed beams, since the sample volume for the high-pressure apparatus is still limited to $\sim 0.04$ cm$^3$, which is over one order of magnitude less than a standard volume of 1 cm$^3$.

Hence, the complementary use of X-ray diffraction is necessary; for example, in exploring experiments of synthetic conditions. It is worth mentioning here that theoretical calculations are also helpful for high-pressure synthetic study because synthesized materials are thermodynamically stable under high pressure and high temperature, and their thermodynamical properties can be predicted theoretically, for instance, by first-principles methods and well examined by comparing the calculated data with the experimental data. In situ X-ray and neutron diffraction measurements combined with first-principles calculations will thus accelerate high-pressure synthetic study of novel hydrides under high pressure.

**Acknowledgments** This work was partially supported by New Energy and Industrial Technology Development Organization (NEDO) under "Advanced Fundamental Research Project on Hydrogen Storage Materials" and "Feasibility Study on Advanced Hydrogen Storage Materials for Automotive Applications (2012)", by the Ministry of Education, Culture, Sports, Science and Technology (MEXT) under the "Photon and Quantum Basic Research Coordinated Development Program", and by Japan Society for the Promotion of Science (JSPS) KAKENHI (25220911, 24241032, and 25420725). The synchrotron radiation experiments were performed at BL14B1 of SPring-8 with the approval of Japan Atomic Energy Agency (JAEA) (2011B3602 and 2012B3602).

## References

1. Fukai Y (2005) The metal–hydrogen system. Springer, Berlin
2. Baranowski B, Filipek SM (2005) 45 years of nickel hydride—history and perspectives. J Alloys Compd 404–406:2–6
3. Filipek SM (2007) Metal hydrides under high hydrostatic pressure. J Adv Sci 19:1–10
4. Filipek SM, Paul-Boncour V, Kuriyama N et al (2010) Hydrides of Laves phases intermetallic compounds synthesized under high hydrogen pressure. Solid State Ion 181:306–310
5. Antonov VE (2002) Phase transformations, crystal and magnetic structures of high-pressure hydrides of d-metals. J Alloys Compd 330–332:110–116
6. Antonov VE, Cornell K, Fedotov VK et al (1998) Neutron diffraction investigation of the dhcp and hcp iron hydrides and deuterides. J Alloys Compd 264:214–222
7. Wakamori K, Filipek SM, Sawaoka A (1983) Convenient method for the synthesis of rare-earth hydrides by the use of a conventional very high pressure technique. Rev Sci Instrum 54:1410
8. Fukai Y, Fukizawa A, Watanabe K et al (1982) Hydrogen in iron—its enhanced dissolution under pressure and stabilization of the γ phase. Jpn J Appl Phys 21:L318–L320

9. Fukai Y, Okuma N (1993) Evidence of copious vacancy formation in Ni and Pd under a high hydrogen pressure. Jpn J Appl Phys 32:L1256–L1259
10. Kyoi D, Rönnebro E, Kitamura N et al (2003) The first magnesium–chromium hydride synthesized by the gigapascal high-pressure technique. J Alloys Compd 361:252–256
11. Moser D, Bull DJ, Sato T et al (2009) Structure and stability of high pressure synthesized Mg–TM hydrides (TM = Ti, Zr, Hf, V, Nb and Ta) as possible new hydrogen rich hydrides for hydrogen storage. J Mater Chem 19:8150–8161
12. Kamegawa A, Goto Y, Kataoka R et al (2008) High-pressure synthesis of novel compounds in an MgNi system. Renew Energy 33:221–225
13. Osugi J, Shimizu K, Inoue K et al (1964) A compact cubic anvil high pressure apparatus. Rev Phys Chem Jpn 34:1
14. Saitoh H, Machida A, Katayama Y et al (2008) Formation and decomposition of $AlH_3$ in the aluminum–hydrogen system. Appl Phys Lett 93:151918
15. Takemura K, Sahu P C, Kunii Y et al (2001) Versatile gas-loading system for diamond-anvil cells. Rev Sci Instrum 72:3873–3876
16. Machida A, Ohmura A, Watanuki T et al (2006) X-ray diffraction investigation of the hexagonal–fcc structural transition in yttrium trihydride under hydrostatic pressure. Solid State Commun 138:436–440
17. Ohmura A, Machida A, Watanuki T et al (2006) Infrared spectroscopic study of the band-gap closure in $YH_3$ at high pressure. Phys Rev B 73:104105
18. Sugimoto H, Fukai Y (1992) Solubility of hydrogen in metals under high hydrogen pressures: thermodynamical calculations. Acta Metall Mater 40:2327–2336
19. Saitoh H, Machida A, Katayama Y et al (2009) Hydrogenation of passivated aluminum with hydrogen fluid. Appl Phys Lett 94:151913–151915
20. Decker DL (1971) High-pressure equation of state for NaCl, KCl, and CsCl. J Appl Phys 42:3239–3244
21. Utsumi W, Funakoshi K, Katayama Y et al (2002) High-pressure science with a multi-anvil apparatus at SPring-8. J Phys: Condens Matter 14:10497–10504
22. Hattori T, Saitoh H, Kaneko H et al (2006) Does bulk metallic glass of elemental Zr and Ti exist? Phys Rev Lett 96:255504
23. Nishihara Y, Funakoshi KI, Higo Y et al (2009) Stress measurement under high pressure using Kawai-type multi-anvil apparatus combined with synchrotron radiation. J Synchrotron Radiat 16:757–761
24. Saitoh H, Okajima Y, Yoneda Y et al (2010) Formation and crystal growth process of $AlH_3$ in Al–H system. J Alloys Compd 496:L25–L28
25. Zhao Y, Zhang J (2008) Microstrain and grain-size analysis from diffraction peak width and graphical derivation of high-pressure themomechanics. J Appl Cryst 41:1095–1108
26. Graetz J, Reilly JJ, Yartys VA et al (2011) Aluminum hydride as a hydrogen and energy storage material: past, present and future. J Alloys Compd 509(Suppl):S517–S528
27. Graetz J, Hauback BC (2013) Recent developments in aluminum-based hydrides for hydrogen storage. MRS Bull 38:473–479
28. Orimo S, Nakamori Y, Kato T et al (2006) Intrinsic and mechanically modified thermal stabilities of α-, β- and γ-aluminum trihydrides $AlH_3$. Appl Phys A 83:5–8
29. Zidan R, Garcia-Diaz BL, Fewox CS et al (2009) Aluminium hydride: a reversible material for hydrogen storage. Chem Commun 25:3717–3719
30. Turley JW, Rinn HW (1969) Crystal structure of aluminum hydride. Inorg Chem 8:18–22
31. Goncharenko I, Eremets MI, Hanfland M et al (2008) Pressure-induced hydrogen-dominant metallic state in aluminum hydride. Phys Rev Lett 100:45504
32. Tkacz M, Filipek S, Baranowski B (1983) High pressure synthesis of aluminum hydride from the elements. Pol J Chem 57:651–653
33. Konovalov SK, Bulychev BM, The P (1995) T-state diagram and solid phase synthesis of aluminum hydride. Inorg Chem 34:172–175
34. Sakharov MK, Antonov VE, Markushkin YE et al (2007) The diagram of phase transformation and phase equilibria in the Al–H system at pressures up to 90 kbar Abstracts of AIRAPT-21 (Catania, Italy), pp 202–203
35. Kato S, Bielmann M, Ikeda K et al (2010) Surface changes on $AlH_3$ during the hydrogen desorption. Appl Phys Lett 96:051912
36. Saitoh H, Machida A, Katayama Y et al (2010) Hydrogen permeation pathways for the hydrogenation reaction of aluminum. J Appl Phys 108:063516
37. Uchida H, Uchida H, Huang YC (1984) Effect of the pulverization of $LaNi_5$ on the hydrogen absorption rate and the X-ray diffraction patterns. J Less-Common Met 101:459–468
38. Saitoh H, Takagi S, Endo N et al (2013) Synthesis and formation process of $Al_2CuH_x$: a new class of interstitial aluminum-based alloy hydride. APL Mater 1:032113
39. Meetsma A, De Boer JL, Van Smaalen S (1989) Refinement of the crystal structure of tetragonal $Al_2Cu$. J Solid State Chem 83:370–372
40. Errandonea D (2010) The melting curve of ten metals up to 12 GPa and 1600 K. J Appl Phys 108:033517
41. Hattori T, Sano A, Arima H et al (2012) BL11: completion of high pressure neutron diffractometer PLANET. MLF Annual report 2011, pp 88–89
42. Hattori T, Sano-Furukawa A, Yamada A et al (2012) BL11: performance of high pressure neutron diffractometer PLANET. MLF Annual report